Detecting Multipath Errors in Terrestrial GNSS Applications

Osechas, O.; Kim, K.J.; Sahinoglu, Z.; Parsons, K.

Abstract

This paper describes a method for detecting multipath errors in satellite navigation services for terrestrial vehicles. The proposed method uses multiple satellite receivers and compares their measurements to detect differences in the rate of change of the carrier phase. The proposed method is tested for nominal operation on real data; faulted operation is studied in two experiments: using real data with an injected fault, and using a simulated signal with an occlusion of the line of sight. In all cases this method outperforms the fault detection capability of a previously existing method, reducing the probability of mis-detecting a given fault by a factor of more than 1010.

Institute of Navigation International Technical Meeting (ITM)

Detecting Multipath Errors in Terrestrial GNSS Applications

Okuary Osechas*[1], Kyeong Jin Kim[2], Kieran Parsons[2], and Zafer Sahinoglu[2]

[2]Mitsubishi Electric Research Lab (MERL), Cambridge, MA

Abstract

This paper describes a method for detecting multipath errors in satellite navigation services for terrestrial vehicles. The proposed method uses multiple satellite receivers and compares their measurements to detect differences in the rate of change of the carrier phase. The proposed method is tested for nominal operation on real data; faulted operation is studied in two experiments: using real data with an injected fault, and using a simulated signal with an occlusion of the line of sight. In all cases this method outperforms the fault detection capability of a previously existing method, reducing the probability of mis-detecting a given fault by a factor of more than 10^{10}.

Introduction

Global Navigation Satellite Systems (GNSS) navigation services for terrestrial vehicles have traditionally been limited to passenger or freight information services, such as pre-trip information, on-trip information, or delivery times, and operations management such as fleet management, cargo monitoring, and maintenance [1]. Control of terrestrial vehicles has, so far, been outside the scope of satellite navigation services. While there is a demand for safety-of-life (SoL) services in the rail industry [1, 2, 3], the challenges in providing high integrity and high availability remain to be significant [4, 5]. The situation is similar in the automotive sector [6, 7, 8, 9].

Some aviation-grade services such as those provided by Satellite-Based Augmentation Systems (SBAS), are capable of delivering the required accuracy [10], but are not designed to provide the required integrity or availability levels in the threat scenario typical of terrestrial users. This leaves users with a choice

---
*The work of O. Osechas was done while he was a Post-Doctoral Researcher at MERL

between adapting the SBAS integrity concept to suit terrestrial applications, or use a completely different approach. One threat to SBAS integrity on land vehicles derives from multipath-induced measurement biases that can go undetected [11]. Unlike aircraft, which operate in tightly controlled environments, terrestrial vehicles are exposed to a variety of multipath-rich scenarios [11]. The disruption of position estimates due to multipath and non-line of sight (NLOS) errors is a potential integrity hazard and needs to be accounted for.

We assume a pair of receivers that are rigidly linked to each other, for example by being mounted on the same vehicle, and have synchronized clocks. We propose a fault monitoring algorithm that works on individual satellite measurements, such that a reported multipath fault leads to the satellite being excluded from the computation of the position solution without making the entire system unavailable. Techniques of this type are also referred to as "channel-wise" tests.

Scenario

In cluttered environments, GNSS receivers may find GNSS satellites to be occluded by features of the surrounding enviornment. In such a case, a NLOS signal might be received from the occluded signal, via reflection on some other feature of the environment (see Figure 1 (a).) This NLOS signal can appear as a valid GNSS signal in the receiver, but the information it carries is invalid, as its propagation path is longer than the LOS. The increase in path length is indicated in Figure 1 (b) with $\Delta r = \Delta r_1 + \Delta r_2$.

The longer path translates into an increase in the time of flight and, therefore, in misleading measurements. Both, code and carrier-phase measurements are, thus, corrupted by systematic errors often referred to as multipath bias.
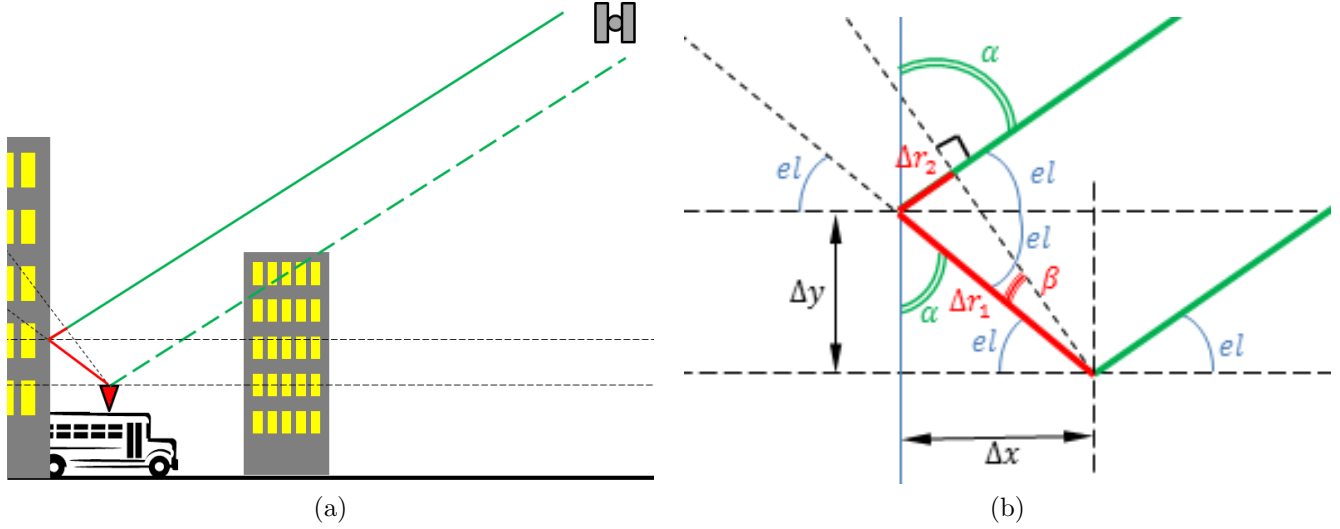
Figure 1: Traveling through urban environments, terrestrial vehicles often find GNSS satellites occluded by buildings. The difference in path length between the LOS distance and the distance traveled by a NLOS signal is indicated in (a), where it is assumed that the distance from receiver to satellite (r) is much greater than the distance from receiver to reflector (Δx), such that the ray from satellite to reflector is parallel to the LOS. A close-up view of the same situation is shown in (b), with some basic angles and relationships indicated.

Prior Solutions: Successive-Time Double Differencing

Basic equations governing GNSS measurements and position estimates are given in [12]. The pseudorange observable for satellite k consists of the true range $r^{(k)}$, which is the difference in position between the satellite and the user $(\mathbf{x}^{(k)} - \mathbf{x}_u)$ projected into the direction of the line of sight $(\mathbf{1}^{(k)} = \frac{\mathbf{x}^{(k)} - \mathbf{x}_u}{\|\mathbf{x}^{(k)} - \mathbf{x}_u\|})$, and the difference between the satellite clock bias $b^{(k)}$ and the user clock bias b_u. The observable also contains random noise $\varepsilon_\rho^{(k)}$ and disturbances such as the ionospheric delay $I^{(k)}$, the tropospheric delay $T^{(k)}$, and the multipath-induced error $M^{(k)}$:

$$\rho^{(k)} = r^{(k)} + b_u - b^{(k)} + I^{(k)} + T^{(k)} + M^{(k)} + \varepsilon_\rho^{(k)}. \quad (1)$$

In addition to the pseudorange observable, most GNSS receivers are able to detect the carrier signal and measure its phase, which yields a more precise but ambiguous measurement than $\rho^{(k)}$

$$\varphi^{(k)} = r^{(k)} + b_u - b^{(k)} - I^{(k)} + T^{(k)} + m^{(k)} + \lambda N^{(k)} + \varepsilon_\phi^{(k)}, \quad (2)$$

where $N^{(k)}$ is the integer ambiguity, and λ is the wavelength of the carrier signal.

The challenge of detecting multipath errors on GNSS measurements has been tackled by a number of different research groups. One successful approach is based on Successive-Time Double Differences (STDD) [13]. Here code (ρ) and carrier-phase (ϕ) measurements

are combined at time steps t_0 and t_1, to make the multipath bias $M^{(k)}$ observable:

$$STDD = \left(\rho_{t1}^{(k)} - \varphi_{t1}^{(k)}\right) - \left(\rho_{t0}^{(k)} - \varphi_{t0}^{(k)}\right) =$$
$$= \left(M_{t1}^{(k)} - M_{t0}^{(k)}\right) - \left(m_{t1}^{(k)} - m_{t0}^{(k)}\right) +$$
$$+ 2\left(I_{t1}^{(k)} - I_{t0}^{(k)}\right) - \lambda\left(N_{t1}^{(k)} - N_{t0}^{(k)}\right) + \nu_{t1,t0}^{(k)}. \quad (3)$$

In equation (3) the noise term $\nu_{t1,t0}^{(k)} \triangleq (\varepsilon_{\rho,t1}^{(k)} - \varepsilon_{\rho,t0}^{(k)}) - (\varepsilon_{\phi,t1}^{(k)} - \varepsilon_{\phi,t0}^{(k)})$ collects the random noise on the observables in one term.

The authors assume that changes in the ionosphere are much slower than changes in $M^{(k)}$, that $m^{(k)} \leq 2\pi$, and that there are no undetected cycle slips ($N_{t1}^{(k)} = N_{t0}^{(k)}$). Under these assumptions, and combining the noise terms into $\nu_{t1}^{(k)} = \varepsilon_{\rho,t1} - \varepsilon_{\rho,t0} + \varepsilon_{\phi,t1} - \varepsilon_{\phi,t0}$, equation (3) becomes:

$$\left(\rho_{t1}^{(k)} - \phi_{t1}^{(k)}\right) - \left(\rho_{t0}^{(k)} - \phi_{t0}^{(k)}\right) + \nu_{t1}^{(k)} =$$
$$= \left(M_{t1}^{(k)} - M_{t0}^{(k)}\right) + \nu_{t1,t0}^{(k)}. \quad (4)$$

Although the resulting channel-wise monitor is sensitive to multipath errors, it has two shortcomings. For one, STDD is computed from code-based pseudorange measurements (which are noisier than carrier-phase measurements), and for another, its reliance on successive measurements introduces correlation into

the random component. The monitor proposed in our work addresses these shortcomings by using carrier-based measurements only, and by using a snapshot method that reduces the time correlation between measurements.

Our Solution: Spatial Difference in Phase Rate

We define the monitoring statistic $mp^{(k)}$ as the difference in the rate of change of the carrier phase ($\dot{\varphi}$) at two distinct locations (A, B) on one vehicle:

$$mp^{(k)} = \dot{\varphi}_A^{(k)} - \dot{\varphi}_B^{(k)}. \quad (5)$$

This quantity will react to the presence of multipath-induced biases on the ranging measurements to satellite k. As indicated before, $mp^{(k)}$ is designed to require only carrier-phase measurements ($\varphi^{(k)}$). The measurement model for $\varphi^{(k)}$ can be adapted from [12] as:

$$\varphi^{(k)} = \left(\mathbf{x}^{(k)} - \mathbf{x}\right) \cdot \mathbf{1}^{(k)} + b_u - b^{(k)} + m^{(k)} + \varepsilon_\phi^{(k)}. \quad (6)$$

Taking the first derivative, the expression for the Doppler frequency on satellite k becomes:

$$\dot{\varphi}^{(k)} = \left(\mathbf{v}^{(k)} - \mathbf{v}\right) \cdot \mathbf{1}^{(k)} + \dot{b}_u - \dot{b}^{(k)} + \dot{m}^{(k)} + \varepsilon_{\dot{\phi}}^{(k)}. \quad (7)$$

Now for two identical receivers that are rigidly linked and have synchronized clocks, the difference in $\dot{\phi}$ will be:

$$mp^{(k)} = \left(\mathbf{v}^{(k)} - \mathbf{v}_A\right) \cdot \mathbf{1}_A^{(k)} - \left(\mathbf{v}^{(k)} - \mathbf{v}_B\right) \cdot \mathbf{1}_B^{(k)} +$$

$$+ \dot{b}_A - \dot{b}_B - (\dot{b}^{(k)} - \dot{b}^{(k)}) + \dot{m}_A^{(k)} - \dot{m}_B^{(k)} + \varepsilon_{\dot{\varphi},A}^{(k)} - \varepsilon_{\dot{\varphi},B}^{(k)}. \quad (8)$$

Here we make the following assumptions about the system requirements:

- Two rigidly linked, kinematically constrained receivers, such their velocities are equal: $\mathbf{v}_A \approx \mathbf{v}_B$, assuming that due to the kinematic constraints the rotation rate is small enough to be neglected.

- The two receiver clocks are synchronized, then $\dot{b}_A \approx \dot{b}_B$.

- Differences in ionospheric and tropospheric delay rates between the two receivers are negligibly small: $\dot{I}_A \approx \dot{I}_B$, $\dot{T}_A \approx \dot{T}_B$.

- The two receivers are identical, such that Doppler measurement noise is zero-mean Gaussian, which yields $\varepsilon_{\dot{\varphi}} \sim \mathcal{N}(0, \sigma_{\dot{\varphi}})$ and therefore $\varepsilon_{SDPR}^{(k)} = \varepsilon_{\dot{\varphi},A}^{(k)} - \varepsilon_{\dot{\varphi},B}^{(k)} \sim \mathcal{N}(0, \sqrt{2}\sigma_{\dot{\varphi}})$.

Under these considerations, equation (8) can be simplified to:

$$\dot{\varphi}_A^{(k)} - \dot{\varphi}_B^{(k)} = \dot{m}_A^{(k)} - \dot{m}_B^{(k)} + \varepsilon_{SDPR}^{(k)}. \quad (9)$$

Fault Model

The multipath scenario, described above, affects the GNSS observables in different ways. This effect can be modeled by deriving the trigonometric relationship of the increase in path length as a function of the horizontal distance between antenna and reflector (Δx) and the elevation angle of the satellite (el). The model can be derived from geometric considerations on Figure 1:

$$\Delta r = f\left(\Delta x, el\right). \quad (10)$$

As defined in Figure 1 (b), it is immediately apparent that $\Delta r_1 = \frac{\Delta x}{\cos(el)}$ and $\Delta r_2 = \Delta r_1 \cos(2\,el)$, which leads to:

$$\Delta r = 2\,\Delta x\,\cos(el). \quad (11)$$

Now, the range rate difference in this changing geometry becomes:

$$\frac{d}{dt}(\Delta r) = 2\,\frac{d}{dt}(\Delta x)\,\cos(el) - 2\,\Delta x\,\sin(el)\frac{d}{dt}(el). \quad (12)$$

From equation (12) it follows that $\frac{d}{dt}(\Delta r)$ can have any instantaneous value, regardless of the value of Δr.

Fault Profile: tanh Blendover

In a cluttered terrestrial environment, one conceivable fault scenario could be to have a strong LOS signal, at the same time as a weak NLOS reflection; then as the vehicle moves through the environment, the LOS signal might be occluded in a smooth transition to zero. This would leave the receiver with only the NLOS signal, which is likely to have a different phase than the LOS signal.

The phase of the received signal would then transition from an initial phase, resulting from the sum of LOS and NLOS signals, to the phase of the NLOS signal on its own.

One possibility for modeling the smooth transition of the LOS from full amplitude to zero is to use a tanh-like behavior:

$$S_{\text{LOS}} = \frac{1}{2}\left(1 - \tanh(\frac{t - t_0}{\Delta t})\right) e^{j\omega t}, \quad (13)$$

where S_{LOS} is the power of the LOS signal, t_0 is the fault onset, and ω is the carrier frequency of the received LOS signal.

In accordance with equation (13), the code-based measurements ($\rho^{(k)}$) are assumed to be affected with a smooth transition around t_0, as the receiver goes from tracking the LOS signal to tracking the NLOS.
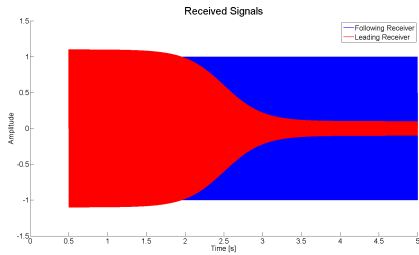
Figure 2: Time-domain plot of the two received signals at the receivers during a multipath fault. The red curve represents the faulted receiver, where the LOS component fades out and a NLOS component remains. The blue curve shows the unaffected receiver with a constant signal amplitude and phase.

For this implementation, no particular geometry is assumed explicitly, but the behavior does conform to equation (10), where the LOS signal fades out and a background NLOS component remains; the corresponding time-domain signals are shown in Figure 2. In such a scenario the carrier phase has a steady jump, while the carrier phase rate (or the Doppler frequency) experiences a spike.

In this case, the received signal would be the sum of the LOS signal S_{LOS} and the NLOS signal $E(t) = Ae^{j(\omega+\Delta\omega)(t+\tau)}$, leading to a received signal of:

$$\frac{1}{2}\left(1 - \tanh\left(\frac{t-t_0}{\Delta t}\right)\right)e^{j\omega t} + Ae^{j(\omega+\Delta\omega)(t+\tau)} =$$

$$= S(t) + E(t)e^{j\varphi(t)} = \tilde{A}e^{j\omega(t)t+\theta_{in}(t)}, \qquad (14)$$

where $\tilde{A}$ is the amplitude of the received signal and θ_{in} is the phase of the received signal. Under this definition, the phase becomes:

$$\theta_{in} = \tan^{-1}\left(\frac{E(t)\sin(\phi(t))}{S(t) + E(t)\cos(\phi(t))}\right). \qquad (15)$$

To better illustrate the difference, Figure 3 shows the expected behavior of the carrier phase and carrier phase rate readings at each receiver, as they enter a multipath fault. Here it is assumed that they are moving on a train car and that receiver A enters the faulted zone before receiver B does.

In this light, the response of the monitoring to the situation depicted in Figure 2 leads to the monitor response shown in Figure 4.

One important observation from these plots is the fundamental difference between the phase responses and the phase rate responses. While the phase jumps,
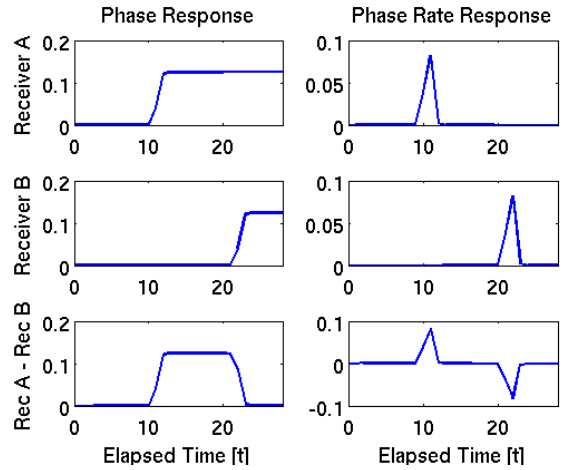

Figure 3: A summary of the expected behavior of two receivers entering a multipath environment shortly after one another. The left column shows the behavior of the carrier phase for each receiver and their difference, while the right column shows the phase rate at the same locations. The top row shows the expected behavior for receiver A, the middle row for receiver B, and the bottom row shows the difference of the two signals.

and the corresponding difference, will be bounded some maximum value, regardless of the transition time, the phase rate and phase rate difference will show an increasingly stronger spike as the transition time is reduced. This observation prompted a study of the detectability of faults with this profile, as a function of the transition time.
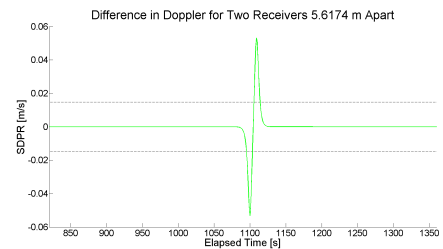

Figure 4: The injected fault for the scenario described by equation (13); the carrier-phase rate of change behaves in accordance with equation (15).

Prototype Implementation

To study the performance of the multipath monitor we used data made available by the CORS network [14].

Specifically, we downloaded data from the receiver stations at sites ZOA1 and ZOA2, located in Oakland, California. These two sites are 5.6 m apart from each other, providing a short enough baseline for the SDPR monitor to work. Note that on a real vehicle, the two receivers would likely be further apart than 5.6 m, but the problem becomes more challenging with shorter baselines. Having a shorter baseline means that the time during which a multipath fault causes a difference in $\dot{\varphi}$ between the two receivers is shorter, so this test setup is actually conservative considering that typical busses, trucks, or train cars are longer than 6 m. The data provided are sampled at 1 Hz over a period of two hours; measurements of code and carrier are available at the L1 frequency; the receiver clocks are Cesium standards [15] and are well behaved enough that the method worked without having to synchronize the clock rates.

Due to the nature of the data, the Doppler frequency was approximated by taking the numerical derivative of adjacent carrier-phase samples. Note that this contradicts the assumptions of of the fault model and introduces a small degree of correlation into the data. This degree of correlation, however, has turned out to be negligible compared to effects that appear in the STDD monitor upon the inclusion of code-based measurements. The results of the experiment are shown in Figure 5(a).

In order to show the benefits of the SDPR monitor over STDD, we injected the same fault shown in Figure 4 into the $\rho^{(k)}$ and $\phi^{(k)}$ measurements that make up STDD. The resulting monitor behavior, shown in Figure 6(b), does not indicate the presence of the injected multipath fault. This can be seen from the fact that the behavior of the monitor is unchanged during the time in which the fault manifests itself in the measurements (between 500 s and 2000 s).

Injected Fault

Applying the previously described fault model to the CORS measurement data requires injecting disturbances into the code and carrier-phase measurements. By injecting disturbances of known magnitude, we are able to quantify the response of SDPR, and therefore predict its behavior in different mulipath scenarios.

The fault profile was chosen in accordance with the scenario described by equation (13), under the assumption that a fault would first affect one receiver, then the other. The multipath fault was injected into both, the code-based pseudorange measurements, and the carrier-phase measurements; this provides a way

of comparing the response of the STDD monitor with SDPR.

Figure 3 shows how the fault would manifest itself, if no other disturbances were present, in particular no measurement noise.

Monitor Response

The responses of SDPR and STDD to the injected fault profile behave as expected: the SDPR response behaves as predicted by equation (15), while STDD behaves as equation (13). The responses are shown in Figure 4, where it is apparent that SDPR provides better detectability than does STDD.

The difference in detectability stems from the fact that the response in SDPR is due to a spatial difference in the frequency of the received signal, while STDD reacts to changes in pseudorange measurements over time. Note that the way carrier-phase measurements are used in STDD assumes that they are inherently less sensitive to multipath than code measurements.

In addition to the lower noise floor on the carrier-based measurements, there is a fundamental difference in the fault response: the multipath fault maps into the range measurement as a difference in path length, and so detection methods based on pseudorange observables ($\rho^{(k)}$) will change by only that amount. In contrast, monitoring the rate of change of the carrier phase ($\dot{\phi}^{(k)}$) is equivalent to observing the time derivative of the range error; thus, a fast-changing multipath disturbance causes a stronger monitor response.

To better understand the detectability of fast multipath faults with SDPR under the fault model of equations (13) - (15), we have tested a range of different operating conditions by sweeping through the relevant parameters: the amplitude of the NLOS signal E and the transition time Δt. The amplitude of E is important as it directly influences the phase difference between the LOS and NLOS signals, while Δt drives the response of $\dot{\theta}$: a fast transition has a higher rate of change than a slow transition, and is therefore more observable using SDPR.

Fault detectability can be assessed using the probability of detection of a given fault. For that purpose we define a detection threshold, set for a constant rate of false alerts (for our case: 10^{-5} false alerts per hour). For a fault of known magnitude, the probability of detection is the cumulative probability above the detection threshold of the faulted distribution. For this
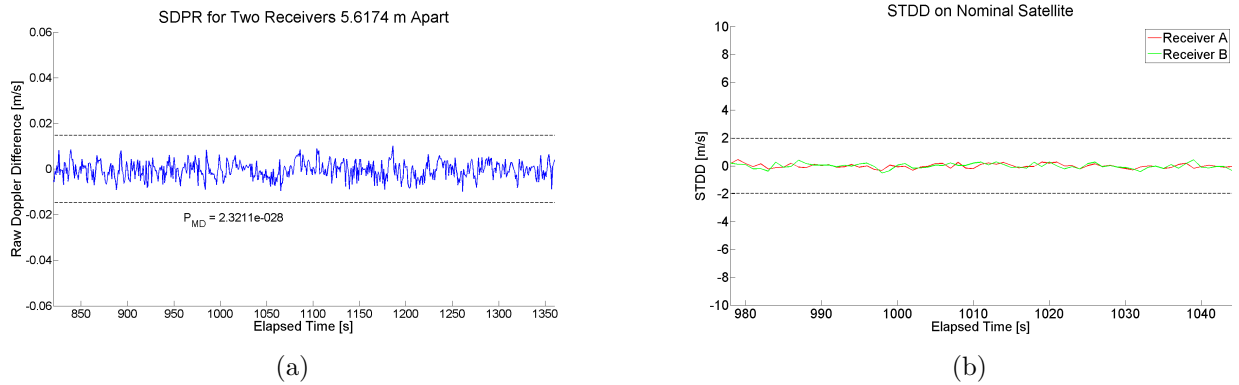
Figure 5: (a) The SDPR monitor under no-fault circumstances. The detection thresholds, computed for a Gaussian model at 10^{-5} false alerts per hour, are indicated by black dashed lines. (b) The STDD monitor under no-fault circumstances.
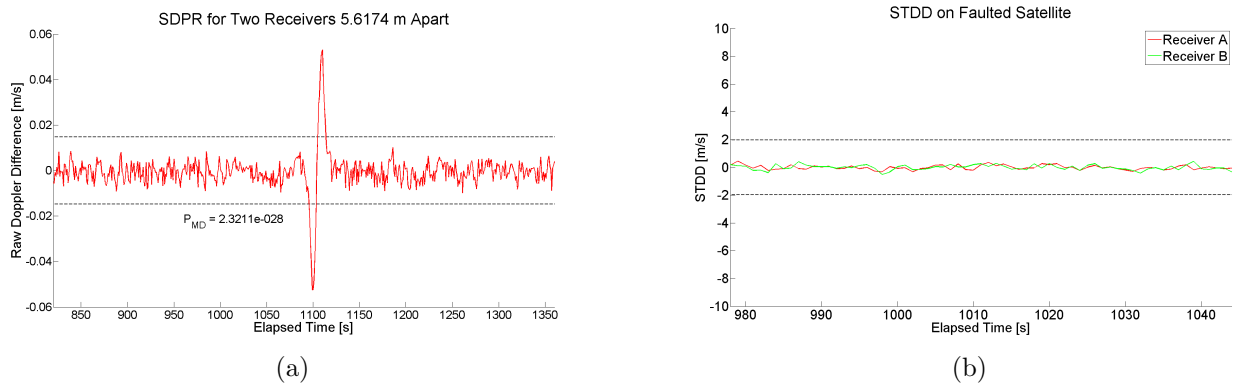

Figure 6: (a) Response of the SDPR monitor during the fault shown in Figure 4. The limits on the horizontal axis were selected for best readability, parts of the monitor response are not shown. The monitor is able to detect a multipath fault of 13 cm and a maximum multipath rate of 3.6 cm/s with an estimated probability of $1 - 1.14 \, 10^{-8}$. (b) The faulted behavior of the STDD monitor applied to the data in question does not show a significant peak at fault time. The STDD monitor is not able to reliably detect the fault of Figure 4.
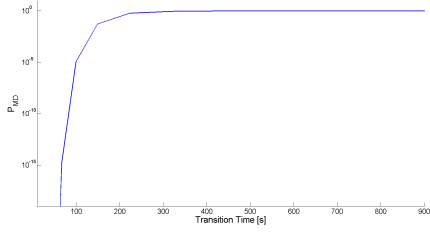
Figure 7: Probability of Mis-Detection (P_{MD}) vs. transition time. Varying the time it takes for the incoming signal to transition from LOS to NLOS, in accordance with equation (13), affects the detectability of multipath faults with SDPR. For transition times shorter than $100\,s$ the multipath fault of equation (13) is detectable in 99.999% of cases, which shos that fast faults are more reliably detected than slower ones.

case the distribution is a Gaussian function, where the mean value corresponds to the multipath rate and the standard deviation is that of the background noise on the monitoring statistic mp. For a more detailed description of how to compute the probability of mis-detection under more general circumstances please refer to [16] or [17].

Simulation

Given the difficulties involved in collecting accurate data on GNSS multipath measurements from fast-moving receivers, such as those in terrestrial transportation, we have resorted to simulated measurements to better characterize the behavior of SDPR under faulted conditions.

The data set used in studying the fault-detection capability of SDPR were generated from a commercial GNSS simulator [18] and processed using a software receiver [19]. This allowed some degree of control in designing the simulated setup, but full access to a typical GNSS processing chain.

Simulated Scenario

The data were generated by simulating a stationary receiver at a pre-defined location. At the begining of the simulation the receiver has eight satellites in view (all-in-view geometry). At time t_1 a set of buildings appears suddenly, blocking the lines of sight to five satellites, but providing a reflection for one satellite, as depicted in Figure 8. This reflection is such that the satellite continues to be tracked by the receiver,

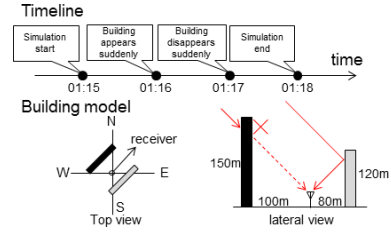leading to a NLOS fault situation similar to that of equation (15).

Figure 8: The simulated multipath fault blocks the LOS from receiver to PRN 22.

Nominal Behavior

In the case where no multipath faults were present in the generation of simulated measurements, both multipath monitors behave as expected: no significant bias and a standard deviation that does not seem to vary significantly over time. Figure 9 shows that both SDPR and STDD are, in this sense, well-behaved monitors.

The sensitivity of any fault monitors depends on the nominal behavior of the data, shown in Figure 9. Specifically, a monitor with a small standard deviation and a small mean value will provide better detection performance. For these data, the values are:

	μ	σ
STDD:	$< 10^{-13}\ m/s$	$32.8 \times 10^{-3}\ m/s$
SDPR:	$12 \times 10^{-3}\ m/s$	$8.60\ m/s$

Table 1: Nominal Behavior of STDD and SDPR

Faulted Behavior

A reading of the faulted behavior shown in the graphs of Figure 9 shows that SDPR provides better fault detectability than STDD, for the given fault profile. This can be attributed to the higher ratio of the peak monitor excursion to nominal noise observed in SDPR. Table 2 summarizes the response of both STDD and SDPR to the same simulated multipath fault.
The results displayed in Figure 9 and summarized in Table 2 support the hypothesis that SDPR provides better detection performance for multipath faults than STDD does.
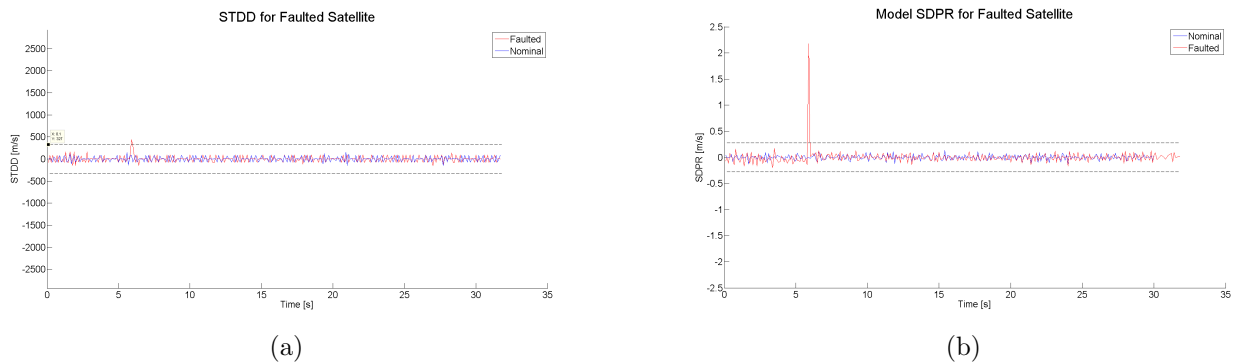
(a)　　　　　　　　　　　　　　　　(b)

Figure 9: Comparison of response under nominal circumstances (blue curves) and multipath fault (red curves) for STDD (a) and SDPR (b). Both figures indicate a detection threshold, computed for a probability of false alert of 10^{-5} per hour.

	$\frac{mx}{\sigma_m}$	P_{MD}
STDD:	9.18	2.3×10^{-2}
SDPR:	37.03	$< 10^{-20}$

Table 2: Fault Response of STDD and SDPR

Discussion

Using spatially separated, rigidly connected GNSS receivers and monitoring differences in the rates of change in the carrier-phase observables has proven to be beneficial in monitoring GNSS signals for multipath-induced disruptions. This method is shown to have superior detection performance over a previously existing method (STDD [13]), partly due to its independence from code-based pseudorange measurements.

In addition to providing a lower level of background noise, SDPR can also respond faster than STDD. A method that responds more quickly to multipath-induced errors is particularly useful for fast-moving urban and sub-urban applications. While STDD requires the computation of pseudorange observables, SDPR does not. For a given PRN, SDPR can be computed directly from the difference in frequency of the two received signals. This allows SDPR to be computed as often as every microsecond, or even more often, rather than every millisecond. Providing this kind of observable, however, may require modifications to the processing chain in the GNSS receiver, as carrier wave and PRN code would need to be tracked separately.

The profile of the multipath disturbance and its behavior over time depend heavily on the physical location at which multipath occurs. For a method that relies on the time derivative of a quantity, as SDPR does, it is particularly important to have a model for how that quantity evolves over time, such as θ_{in} in equation (15). The behavior over time is influenced by the trajectory of the moving vehicle, the outline of the obstacles occluding the LOS, the shape and orientation of reflecting surfaces providing NLOS propagation, and the satellite geometry among other factors. The choice of a tanh-like profile for the amplitude of the LOS signal and the constant amplitude of the NLOS signal represents a simplification of a complex situation, but provides enough flexibility to allow an assessment of the most significant influences on the fault detection mechanism.

Another consequence of monitoring the time derivative of the carrier phase is that SDPR is more sensitive on fast-moving vehicles than on slow-moving vehicles. In a faster vehicle, the transition time, Δt in equation (13), is shorter than in a slower vehicle traveling through the same environment. The results of Figure 7 show that faults are more likely to be detected by SDPR as the transition time decreases, making this a very effective method for vehicles traveling at high speeds.

Summary

Providing reliable monitoring for multipath faults in terrestrial environments may enable safety-of-life services to be deployed to terrestrial applications of satellite navigation. This paper introduces a method for detecting changes in the multipath environment as typically experienced by a terrestrial user of satellite navigation services. The method is based on observing the spatial difference of the

rate of change in the signal received from each satellite.

A prototype implementation of the method was tested for nominal operation with real data, gathered from the CORS service; the fault response of the same prototype is tested using a synthetic fault model. The results show that the new method is more sensitive to changes in the multipath environment than prior art.

A more refined version of the method was then tested for detection performance using data from a signal emulator, where the multipath fault is generated by simulating an occlusion of the line of sight and non-line-of-sight reception of the signal. Under these circumstances the proposed approach has been shown to outperform the existing method.

References

[1] J-M. Wiss, G. Barbu, Frosig, M. Schröder, C. Edwards, K. Walter, A. Filip, A. Sage, and S. Forsyth, "Requirements of Rail Applications," Technical report, GNSS Rail User Forum, 2000.

[2] Juliette Marais and Julie Beugin, "Evaluation Method of GNSS-based Positioning Functions for Safety Applications in Operational Conditions ," *Procedia - Social and Behavioral Sciences*, vol. 48, no. 0, pp. 806 – 815, 2012, Transport Research Arena 2012.

[3] Federal Railroad Administration, "Positive Train Control Systems; Final Rule," Federal Register, January 2010.

[4] L. Marradi, A. Galimberti, L. Foglia, A. Zin, C. Pecchioni, M. Doronzo, E.J. Gonzalez Garcia-Consuegra, and M. Lekchiri, "GNSS for Enhanced Odometry: The GRAIL-2 results," in *Satellite Navigation Technologies and European Workshop on GNSS Signals and Signal Processing, (NAVITEC), 2012 6th ESA Workshop on*, Dec 2012, pp. 1–7.

[5] Boubeker Belabbas and Anja Grosch, "Novel Integrity Monitoring for Train Navigation using a GNSS-IMU Bayesian Position Estimator and a Curvature Change Detector," in *ION GNSS+*, 2013.

[6] H. Beckmann, V. Kropp, and B. Eissfeller, "New Integrity Concept for Intelligent Transportation Systems (ITS) for Safety of Live (SoL) applications," in *Position, Location and Navigation Symposium-PLANS*. IEEE, 2014, pp. 982–988.

[7] R. Toledo, M.A. Zamora, B. Ubeda, and A.F. Gomez-Skarmeta, "An Integrity Navigation System Based on GNSS/INS for Remote Services Implementation In Terrestrial Vehicles," in *Intelligent Transportation Systems, 2004. Proceedings. The 7th International IEEE Conference on*, Oct 2004, pp. 477–480.

[8] R. Garcia, T. de Pedro, J.E. Naranjo, J. Reviejo, and C. Gonzalez, "Frontal and Lateral Control for Unmanned Vehicles In Urban Tracks," in *Intelligent Vehicle Symposium, 2002. IEEE*, June 2002, vol. 2, pp. 583–588 vol.2.

[9] David M Bevly and Stewart Cobb, *GNSS for Vehicle Control*, Artech House, 2010.

[10] RTCA Inc., "Minimum Operational Performance Standards for Global Positioning System/Wide Area Augmentation System Airborne Equipment," 2012.

[11] Andreas Lehner and Alexander Steingass, "A Novel Channel Model for Land Mobile Satellite Navigation," in *Proceedings ION ITM*, 2005.

[12] Pratap Misra and Per Enge, *Global Positioning System: Signals, Measurements and Performance Second Edition*, Massachusetts: Ganga-Jamuna Press, 2006.

[13] Hyung Keun Lee, Jang Gyu Lee, and Gyu-In Jee, "GPS Multipath Detection Based on Sequence of Successive-Time Double-Differences," *IEEE Signal Processing Letters*, vol. 11, no. 3, pp. 316–319, 2004.

[14] Richard Snay, "The National and Cooperative CORS Systems in 2000 and Beyond," in *Proceedings of ION GPS*, 2000, vol. 55, p. 2000.

[15] "ZOA1 Site Information Form," `http://www.ngs.noaa.gov/cgi-cors/corsage_2.prl`, 08 2013.

[16] Jason Rife, "Influence of GNSS Integrity Monitoring on Single and Multiple Fault Event Probabilities," *ION GNSS 2008*, pp. 16–19, 2008.

[17] Okuary Osechas, Pratap Misra, and Jason Rife, "Carrier-Phase Acceleration RAIM for GNSS Satellite Clock Fault Detection," *Navigation*, vol. 59, no. 3, pp. 221–235, 2012.

[18] Spirent Communications, "GNSS Engineer's Handbook. Application Note DAN004-TM," Whitepaper, 2014.

[19] Kai Borre, Dennis Akos, Nicolaj Bertelsen, Peter Rinder, and Soren Holdt Jensen, *A Software-Defined GPS and Galileo Receiver: Single-Frequency Approach. A Single-Frequency Approach*, Birkhäuser Boston, 2007.